IEEE Access
Multidisciplinary | Rapid Review | Open Access Journal

Received 9 September 2025, accepted 25 October 2025, date of publication 30 October 2025, date of current version 5 November 2025.

Digital Object Identifier 10.1109/ACCESS.2025.3627080

RESEARCH ARTICLE

Magnetization Losses and Non-Reduced 3D Modeling of Hybrid CORC-TSTC Composite Conductors

HASAN N. H. AL-SSALIH[1,2], MATTHEW CLEGG[1,3], ANTONIO BADÍA-MAJÓS[4], AND HAROLD S. RUIZ[1]

[1]School of Engineering and Space Park Leicester, University of Leicester, LE1 7RH Leicester, U.K.
[2]Electrical Engineering Division, Southern Fertilizer State Company, Khor Al-Zubair, Basrah Governorate 61025, Iraq
[3]U.K. Power Networks, SE1 6NP London, U.K.
[4]Instituto de Nanociencia y Materiales de Aragón (INMA), CSIC-Universidad de Zaragoza, 50009 Zaragoza, Spain

Corresponding author: Harold S. Ruiz (dr.harold.ruiz@leicester.ac.uk)

This work was supported in part by U.K. Research and Innovation (UKRI), Engineering and Physical Sciences Research Council (EPSRC), led by Harold S. Ruiz under Grant EP/S025707/1; and in part by European Cooperation in Science and Technology through European Cooperation in Science and Technology (COST) Action (Hi-SCALE, https://www.cost.eu/actions/CA19108/ and https://hi-scale.eu/) under Grant CA19108. The work of Hasan N. H. Al-Ssalih was supported by Iraq's Higher Committee for Education Development (HCED). The work of Matthew Clegg was supported by the University of Leicester and the EPSRC Doctoral Training Program under Grant EP/2438289. The work of Antonio BadÍa-Majós was supported in part by Ministerio de Ciencia, Innovación y Universidades (MICIU) and the Agencia Estatal de Investigación (AEI) under Grant MICIU/AEI/10.13039/501100011033, and the European Regional Development Fund (ERDF) under Project PID2023-146041OB-C21, and in part by Gobierno de Aragón under Grant T54-23R.

ABSTRACT The Conductor on Round Core (CORC) and Twisted Stacked-Tape Conductor (TSTC) are among the most promising architectures for high-temperature superconducting (HTS) cables due to their high current-carrying capabilities, essential for future fusion and high voltage -high current- power applications. While CORC designs offer mechanical robustness, their larger cross-sections can lead to spatial inefficiencies, whereas TSTC cables are more compact but limited in transport current. To bridge these trade-offs, a CORC–TSTC hybrid cable has been recently proposed by Korean researchers, though its electromagnetic performance remains largely unverified. In this work, we present a comprehensive three-dimensional electromagnetic study to validate the experimentally measured AC losses of such hybrid cables, using SuNAM Co. Ltd. GdBCO HTS tapes. Our model captures the full current dynamics on the surface and within the superconducting layers, overcoming the limitations of reduced-order gauge (2D) methods. The hybrid cable configurations considered consist of a six-tape CORC outer layer enclosing a TSTC core with one to four stacked tapes. The model incorporates magneto-angular anisotropy in the critical current density, informed by experimental data, to ensure accurate benchmarking. To contextualize the hybrid design's performance, we also simulate two reference geometries: a single-layer and a double-layer CORC cable, as well as a ten-tape TSTC conductor. Results show that the hybrid configuration offers a compelling balance, combining low AC losses with compact geometry and structural flexibility.

INDEX TERMS Hybrid superconducting cables, CORC–TSTC configuration, AC loss modeling, 3D H-formulation, magnetization currents, GdBCO coated conductors.

I. INTRODUCTION

In the race for developing superconducting cables for applications at large scale, various configurations have been introduced with intricate structural methods and techniques aiming to mitigate the AC losses stemming from the magnetic hysteretic behaviour of type-II superconductors with strong pinning [1]. These losses pose a significant challenge in the development of AC superconducting devices [2], [3], [4], directly impacting the operational efficiency of the cryogenic

The associate editor coordinating the review of this manuscript and approving it for publication was M. Venkateshkumar.

system for the High-Temperature Superconductor (HTS) in power system applications. Unlike long-established power cables [5], HTS cables represent a transformative approach to energy transmission, combining high current-carrying capabilities with minimal power losses and a significantly smaller installation footprint [6]. Their compact form factor makes them particularly advantageous in densely populated or infrastructure-constrained environments, where space limitations hinder the expansion of traditional grid systems [7], [8]. Yet, while the capital investment associated with the procurement of the HTS cables remain higher than those of conventional cables, this is balanced by reduced operational losses, fewer infrastructure upgrades, and improved reliability over time. These factors, along with the continuous progress on already mature cryocooling technology [9], contribute to the growing perception of HTS cables as a long-term, cost-effective solution aligned with energy transition and decarbonisation objectives.

Significant global efforts over the past decade have been directed towards the advancement of HTS cables capable of carrying high currents ranging from tens to hundreds of kilo-Amps. Examples of these cables include, Roebel Assembled Coated Conductor Cables (RACCs) [10], [11], [12], Conductor On Round Core (CORC) cables [13], [14], [15], [16], and the Twisted Stack-Tape Cable (TSTC) [17], [18], [19], being the latter two the ones currently preferred for large scale applications due to their easier manufacturing. CORC cables characterized by a cylindrical core and multiple layers of Rare-earth (Re) Barium cuprates (ReBCO) coated conductors wound helically around it, have consistently demonstrated high power density and mechanical flexibility [14]. Its transposed configuration of superconducting tapes within each layer is known to enhance the effectiveness of the cable by minimizing the current coupling. This technique has been successfully used not only in cables for high field magnets but also for power system cables in single and three phase configurations, whereby increasing the number of tapes and layers, the capacity of transport current increases [17]. Several global efforts and research over the past decade have been directed toward reducing the AC loss characteristics of CORC cables [20], like studies on the effects of magnetic shielding, winding direction and multi-layer layout, and also strategies on the tapes themselves like the investigation of reducing the magnetization loss at a high magnetic field by using striated superconducting tapes [15], [21], [22], [23].

Simultaneously, the other cable design that currently competes with the market for CORC cables is the TSTC conductor, whose cabling technique was initially developed in a single-slot design by Takayasu et al., at MIT in 2012 [18], [24]. Compared to a straightforward cable constructed solely with a stack of untwisted tapes, a TSTC conductor offers various mechanical and electrical benefits [19], [25], including an effective manufacturing cost, tightness, high current density, and partial electromagnetic decoupling [26], where there is no change in the AC losses of the insulated and non-insulated TSTC stacks under applied magnetic field [19]. The fabrication process of a TSTC conductor differs significantly from that of a conventional helically wound HTS power cable, like the CORC design. Consequently, the overall size of the cable can be significantly reduced, aligning the length of the cable closely with that of the HTS tape utilized. This approach results in a notably high efficiency of wire utilization [27] and holds significant utility for both power transmission cables and conductors used in high-field, high-current magnets, including those constructed from cable-in-conduit conductor (CICC) [25], and other forward designs inspired by the TSTC and CORC topologies [28], opening the possibility for the fabrication of hybrid composite conductors.

In the case of hybrid cables, approximate simulation techniques have been employed to estimate AC losses relying on simplified cable geometries, as proposed in [29]. These numerical models are typically based on various formulations of Maxwell's equations, such as the T–A formulation, where gauge conditions are applied to reduce computational complexity at the potential expense of losing physical context. In fact, although mathematically elegant and computationally efficient, from a physical standpoint, gauge-based formulations that reduce either a material-space dimension or the degrees of freedom in the fundamental physical variables are not truly three-dimensional from a physical perspective. As a result, models such as the T-A approach, which approximate the three-dimensional nature of HTS tapes as infinitely thin two-dimensional films, effectively collapsing a 3D physical system into a 2D numerical framework, lack the ability to accurately capture the fundamental physical phenomena of diamagnetism within the HTS tapes [16]. Here, it is worthy to mention that efforts have been made for extending the T-A formulation to 3D scenarios, though as recognized by the authors [30], at the expense of computational burden as compared to other extended methods. In contrast, using the H-formulation with no reduction in the dimension of the system enables the representation of current density profiles across the tape thickness and, thus, allows for a more accurate examination of current distribution. Yet, such models offer an alternative mathematical solution in which the *screening* of magnetic fields mimics diamagnetic behaviour by generating an artificial array of surface ''eddy'' currents [31], [32], [33], [34]. Nonetheless, this does not reflect the actual physical mechanisms at play. In fact, since the early development of the electromagnetic theory for type-II superconductors by the London brothers [35], and supported by the seminal Meissner–Ochsenfeld experiment [36], it has been well established that superconductors do not expel magnetic fields through persistent eddy currents that oppose field penetration. Instead, while screening currents indeed persist at boundaries or around vortices to enforce the Meissner or mixed-state condition, they are generated within the interior of the superconductor, not merely along its surface [37].

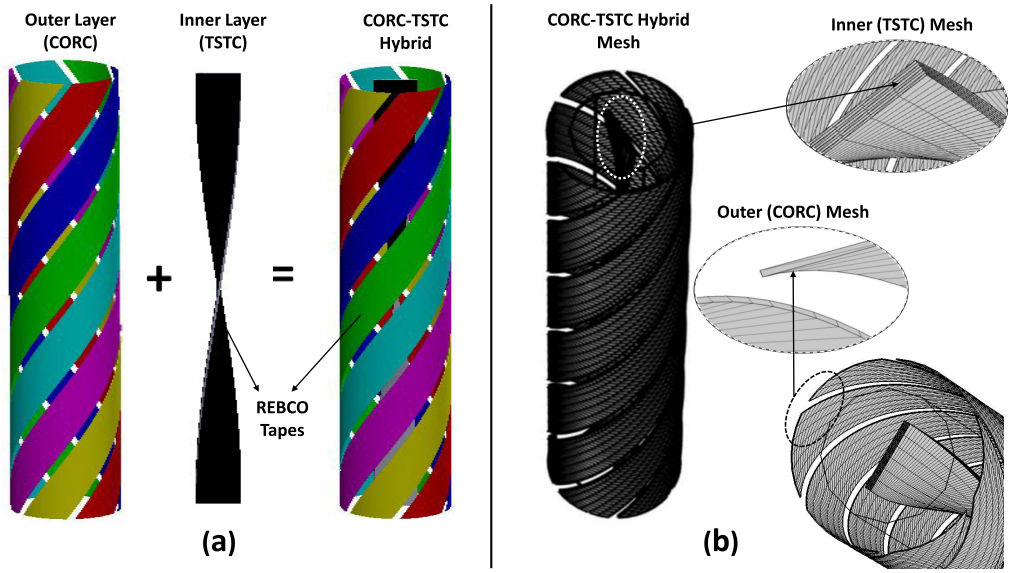

FIGURE 1. Pictorial representation of the CORC-TSTC Hybrid cable showing its (a) composed structure with a CORC outer layer and a TSTC Inner conductor, and (b) the scaled-up ReBCO tape mesh manually tailored within COMSOL. Cable specifications are shown at Table 1.

Thus, considering the world-first experimental measurements of AC losses in the novel CORC–TSTC hybrid cables reported by Yoon et al. [27], in this paper, we present a fully three-dimensional numerical model overcoming the conceptual physical limitations of gauge-reduced formulations, elucidating the actual profiles and local dynamics of current density *inside* the HTS tapes that give rise to the observed AC losses. This builds on our previous success in the electromagnetic modeling of CORC [38] and TSTC [39] cables considered as individual systems, although its implementation is not as simple as the straightforward merging of existing models. This is due to the symmetry breaking between the TSTC and CORC topologies that, when compared under the same physical workplace, particular attention must be paid to the use of adequate meshing techniques with similar elements sizing relative to both wires' dimensioning (see Figure 1).

In particular, we present a detailed study on the impact of increasing the number of stacked layers in the TSTC former, validating our numerical results against the recent experimental observations [27]. Specifically, we investigate the following configurations of HTS tapes within the hybrid CORC–TSTC cables (Figure 1):

1) Six HTS tapes in the CORC layer, and a single HTS tape in the TSTC conductor placed within the CORC former.
2) Six HTS tapes in the CORC layer, and two stacked HTS tapes in the TSTC conductor.
3) Six HTS tapes in the CORC layer, and four stacked HTS tapes in the TSTC conductor.

Additionally, once our computational models are successfully validated against available experimental results for CORC–TSTC hybrid cables, we perform a thorough comparison of their AC losses against equivalent cables with similar HTS tape usage. This includes the electromagnetic performance of single-layer and bilayer CORC cables, as well as TSTC conductors with up to 10 stacked HTS tapes. In all cases, our models retain the full three-dimensional thickness of individual HTS tapes—an important distinction that sets our rigorous approach apart from other studies.

It is worth noting that the CORC–TSTC hybrid cable exhibits a significantly more complex structure compared to its counterparts. For this reason, section II is dedicated not only to summarizing well-known aspects of the H-formulation (Sec. II-A), but more importantly, to discussing the specific considerations required for the successful numerical modeling of hybrid cables. This includes accounting for the strong magneto-angular dependence of the critical current density in HTS tapes (Sec. II-B), the methodology for computing AC losses, and relevant meshing strategies to prevent numerical convergence issues (Sec. II-C). Subsequently, in Sec. III, we present a detailed analysis of the magnetization characteristics of the CORC–TSTC hybrid cable, demonstrating excellent agreement between our simulations and experimental data. This allows us to identify which among the three cable configurations—Hybrid, CORC, or TSTC—yields the lowest hysteretic magnetization losses.

II. METHODOLOGY AND STUDY CONDITIONS

This section outlines the methodology and modeling conditions employed in the numerical analysis of hybrid CORC–TSTC cables. The electromagnetic behaviour of these complex superconducting assemblies is investigated using a fully three-dimensional implementation of the H-formulation, solved through the Finite Element

TABLE 1. General Cable/Tape specifications.

Specification	Value
HTS Tape Manufacturer	SuNAM
HTS Tape Substrate	Hastelloy
Superconductive (SC) Material	GdBCO
SC Film Thickness	0.001 mm
HTS Tape Width	4 mm
HTS Tape Thickness	0.07 mm
HTS Single Tape I_c @ 77 K (*)	190 A
n-Value (*)	42
Hybrid Cable Former Diameter	10 mm
Hybrid Cable Length	90 mm
CORC layer pitch length	90 mm
TSTC layer 0.5pitch length	180 mm
Magneto-Angular Parameters [γ, α, β] (†),	[7.53, 0.02, 0.25]
B_0 parameter (†)	0.0018 T

* Measured at self-field conditions at [40].
† Determined by using the general method for extracting the magneto angular anisotropy of the critical current density of the HTS tapes in [39], [43].

Method (FEM) in COMSOL Multiphysics. Key aspects of the modeling approach, including the governing equations, anisotropic material laws, loss evaluation procedures, and meshing strategies, are discussed in detail across the following subsections.

A. THEORETICAL STATEMENT AND MATERIAL LAW

The numerical model includes six 4 mm-wide HTS tapes forming a single-layer CORC, with an inner TSTC composed of 4 mm SuNAM tapes, each carrying 190 A at 77 K in self-field. All parameters and tape specifications follow the data presented in [27] and [40], which feature experimental measurements of AC losses under a perpendicular 60 Hz sinusoidal magnetic field, with magnitudes ranging from 15 to 100 mT [27]. The initial outer diameter is 10 mm. The prototype CORC (with one twist pitch) and TSTC (with half a pitch) are each 90 mm in length, designed to match the linked pick-up coil (LPC) system for magnetization loss measurement, as described in [27]. The design of the prototyped hybrid cable is illustrated in Figure 1(a), with HTS tape specifications summarized in Table 1.

We have used the widely adopted H-formulation method [41] to simulate the electromagnetic performance of these HTS CORC–TSTC hybrid cables under certain conditions. Firstly, the solution is implemented using the Finite Element Method (FEM) in COMSOL Multiphysics. In this framework, Maxwell's equations in 3D Cartesian coordinates can be formulated as shown in [42], enabling their implementation in the default COMSOL environment without requiring specialized modules. This is achieved via the general PDE interface in COMSOL, represented by:

$$\mathbf{e}_a \frac{\partial^2 \mathbf{H}}{\partial t^2} + \mathbf{d}_a \frac{\partial \mathbf{H}}{\partial t} + \nabla \cdot \Gamma = f \,, \tag{1}$$

where $\mathbf{e}_a$ and $\mathbf{d}_a$ are the so-called mass and damping coefficients, respectively, and Γ is the conservative vectorial flux as defined in COMSOL. The magnetic field $\mathbf{H}$ is expressed as the state variables of the problem in Cartesian coordinates as $\mathbf{H} = [H_x, H_y, H_z]$. The source term $\nabla \cdot \Gamma$ in Equation 1 must be manipulated to match the left-hand side of Faraday's law:

$$\nabla \times \mathbf{E} = -\mu_0 \mu_r \frac{\partial \mathbf{H}}{\partial t} \,, \tag{2}$$

using the same vector notation. To establish a connection between this formulation and the general PDE form, we start by evaluating the divergence of the conservative flux vector $\Gamma = [\Gamma_x, \Gamma_y, \Gamma_z]$, which may account for non-isotropic spatial dependencies. By assuming a zero mass coefficient, $\mathbf{e}_a = 0$, only the damping term $\mathbf{d}_a \partial_t \mathbf{H}$ remains, which is analogous to the right-hand side of Faraday's law, i.e., $\mu_0 \mu_r \partial_t \mathbf{H}$.

The corresponding system of differential equations becomes:

$$\begin{aligned} \frac{\partial E_z}{\partial y} - \frac{\partial E_y}{\partial z} &= -\mu_0 \mu_r \frac{\partial H_x}{\partial t}, \\ \frac{\partial E_x}{\partial z} - \frac{\partial E_z}{\partial x} &= -\mu_0 \mu_r \frac{\partial H_y}{\partial t}, \\ \frac{\partial E_y}{\partial x} - \frac{\partial E_x}{\partial y} &= -\mu_0 \mu_r \frac{\partial H_z}{\partial t}. \end{aligned} \tag{3}$$

Here, the relative magnetic permeability of the superconductor is assumed to be $\mu_r = 1$. In fact, throughout this article, and consistent with typical experimental conditions, we assume that equilibrium magnetization effects in the superconductor are negligible and that no magnetic materials are present. As such, we adopt the approximation $\mathbf{B} \approx \mu_0 \mathbf{H}$. The conductive properties of the material are yet to be defined, so an $E(J)$ law must be introduced. For type-II superconductors, a power-law relation is commonly used [1]:

$$\mathbf{E} = E_0 \left(\frac{\mathbf{J}}{J_c} \right)^n , \tag{4}$$

which resembles Ohm's law in normal conductors, $\rho = |\mathbf{E}|/|\mathbf{J}|$, if one defines an effective resistivity:

$$\rho = \frac{E_0}{J_c}\left|\frac{\mathbf{J}}{J_c}\right|^{n-1}, \tag{5}$$

where E_0 is the critical electric field, typically taken as $0.1\,\mu\mathrm{V\,cm^{-1}}$ in self-field conditions for 2G-HTS tapes [40], n is the power-law exponent, and J_c is the critical current density [1].

The current density $\mathbf{J}$ is obtained from Ampére's law:

$$\nabla \times \mathbf{H} = \mathbf{J}, \tag{6}$$

which in Cartesian coordinates becomes:

$$\begin{aligned} J_x &= \frac{\partial H_z}{\partial y} - \frac{\partial H_y}{\partial z}, \\ J_y &= \frac{\partial H_x}{\partial z} - \frac{\partial H_z}{\partial x}, \\ J_z &= \frac{\partial H_y}{\partial x} - \frac{\partial H_x}{\partial y}. \end{aligned} \tag{7}$$

With these definitions, our physical problem is fully adapted to the general form in Equation 1 and can be readily implemented using FEM in COMSOL Multiphysics. Specifically, the model solves the nonlinear diffusion equation:

$$\nabla \times [\rho\,(\nabla \times \mathbf{H})] = \mu_0 \frac{\partial \mathbf{H}}{\partial t}. \tag{8}$$

Moreover, to ensure numerical convergence and physical validity, additional considerations regarding the dimensionality of the material properties and geometrical configuration of state variables are discussed in the following subsections.

B. ANGLE FORMED WITH APPLIED FIELD

For hybrid cables incorporating helically wound and twisted tapes, establishing the angle θ formed by the magnetic field and the tape's surface is, by no means, as simple as for the case of straight tapes. This is due to the curved layout of the meshed components delineating the superconducting area in a 3D model, and precludes a uniform angle definition across all finite elements.

Thus, when assuming a proper $J_c(B, \theta)$ function for the HTS tapes at Figure 1, unlike for straight tapes, θ varies along the length of the CORC and TSTC conductors, depending on the finite element dimensions composing each of the HTS tapes [16], [43]. This issue can be addressed by introducing a coordinate transformation (local rotation) for the magnetic field components:

$$B'_x = B_x \frac{y}{\sqrt{x^2+y^2}} + B_y \frac{x}{\sqrt{x^2+y^2}}, \tag{9}$$

and,

$$B'_y = -B_x \frac{x}{\sqrt{x^2+y^2}} + B_y \frac{y}{\sqrt{x^2+y^2}}. \tag{10}$$

The spatial coordinate system centre lies in the xy plane at the centre of the CORC cable former, where B_x and B_y represent the magnetic field components measured within the global space coordinate system, which determines the orientation of the local magnetic field. Consequently, the dependence in θ can be addressed using trigonometric identities, such as $\sin\theta = B'_y/|\mathbf{B}|$, $\cos\theta = B'_x/|\mathbf{B}|$. Then, the underlying magneto angular dependence for the coated conductors into the numerical formulation for the CORC-TSTC hybrid cables, $J_c(\mathbf{B}, \theta)$ can be borrowed from the experimentally derived function in [43]:

$$J_c(\mathbf{B}, \theta) = \frac{J_{c0}}{(1 + \epsilon_\theta(|\mathbf{B}|/B_0)^\beta)^\alpha}. \tag{11}$$

Here $\mathbf{B}$ is the calculated local magnetic field vector (applied plus self-field), and J_{c0} is the self-field measured critical current density. The coefficients α, β and B_0 parameterize the thermally activated flux-creep, following the phenomenological work by Kim [44] ($\alpha = 1$, $\beta = 1$ on the original version), and can be established through experimental measurements [39], [45]. Additionally, ϵ_θ represents an anisotropic flux-creep function. This anisotropy in the critical current density J_c arises mainly from the imperfect alignment of the ab-plane of each YBCO grain, with only a small portion of grains having their ab-planes precisely parallel to the tape surface, contributing significantly to inter-grain critical current when the magnetic field is parallel to the tape's surface. Furthermore, the anisotropy is believed to be tailored by the electron mass anisotropy ratio γ of the coated conductor, at least if a macroscopical equation as the one at Equation 11 can be directly derived from experimental observations [43]. As a matter of fact, across the majority of manufacturers of superconducting tapes, the anisotropy function ϵ_θ has been observed to adhere to the following equation [46]:

$$\epsilon_\theta = \sqrt{\gamma^{-1}\sin^2\theta + \cos^2\theta}\ . \tag{12}$$

In our case, the parameters α, β and γ have been obtained by straight computational analysis of experimental data available for the SuNAM tapes in question [39], [45].

C. AC LOSS EVALUATION, SETUP AND MESHING

In our model, a 60 Hz external magnetic field is applied, and the magnetization losses are calculated on a per-cycle basis. Specifically, the AC losses are computed by integrating the local power dissipation density ($\mathbf{E}\cdot\mathbf{J}$) over the volume of the HTS tapes and across one full peak-to-peak hysteretic cycle (denoted as f.c.):

$$Q = \omega \int_{f.c.} dt \int_\Omega \mathbf{E}\cdot\mathbf{J}\, d\Omega. \tag{13}$$

Here, ω is the angular frequency of the externally applied magnetic field, and Ω denotes the volume of the SC sample.

To ensure accuracy, the AC loss calculation begins from the second quarter-cycle of the applied magnetic field, in order to exclude the effects of the initial magnetization transient in the first half-cycle [34]. A full assessment of AC losses in the CORC–TSTC hybrid cable, across the range of magnetic field amplitudes from 15 mT to 100 mT, is presented

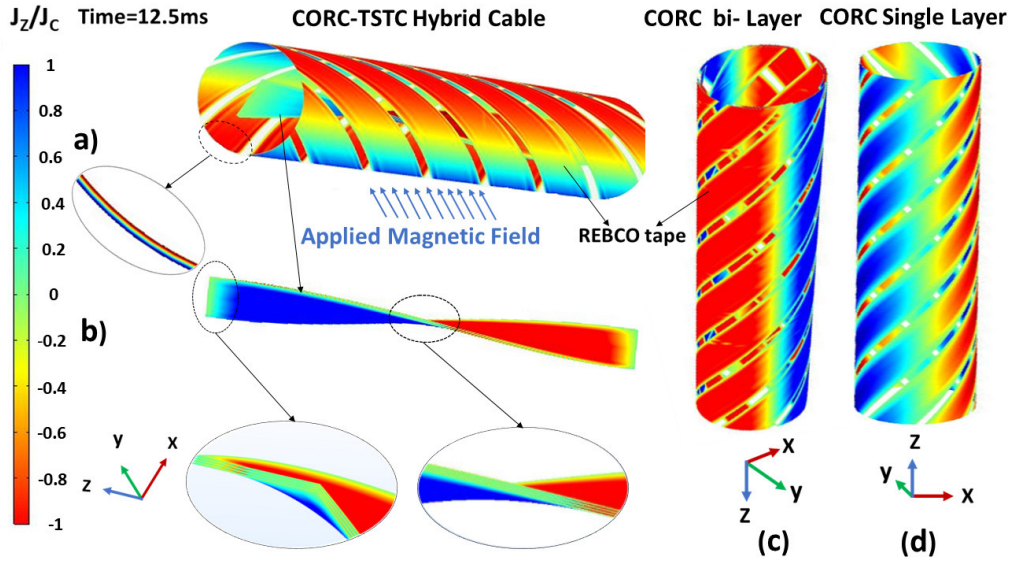

FIGURE 2. Distribution of normalized current density, J_z/J_c, in hybrid CORC–TSTC cables. (a) hybrid configuration consisting of six HTS tapes in the CORC layer and four tapes in the inner TSTC conductor. A zoomed-in cross-sectional view of a 2G-HTS tape reveals magnetization currents satisfying Ampére's law, along with a clearly defined flux-free core—an internal structure not visible through other 3D modeling techniques.(b) Corresponding current density profiles in the inner TSTC conductor evaluated after 12.5 ms under an applied AC magnetic field $B = B_{ac}\sin(\omega t)$, with an amplitude of $B_{ac} = 90$ mT oriented along the y-axis.(c) Configuration of a two-layer CORC cable composed of 10 HTS tapes.(d) Configuration of a single-layer CORC cable composed of 6 HTS tapes.

in Sec. III-B. Furthermore, due to the complex structure of the hybrid cable (Figure 1), developing a numerical model that can efficiently and accurately capture its operational performance, considering the high width/thickness ratio of the SC film within each of the HTS tapes (see Table 1), poses a significant challenge. In this work, to overcome numerical difficulties arising from the large aspect ratio of the second-generation high-temperature superconducting (2G-HTS) tapes, the 1 μm thickness of the 4 mm-wide ReBCO layer in the 2G-HTS tapes used was scaled up by a factor of 50 (see Figure 1(b)). Simultaneously, the critical current density J_c of the superconducting layers was renormalized by the same factor. This scaling approach addresses the computational difficulties caused by the extreme aspect ratio of the tapes while maintaining the model's accuracy to a considerable extent, as shown by numerous prior studies [47], [48], while maintaining a valid physical picture for the distribution of current density on the surface an the inside of the HTS tapes (see Figure 2 & Figure 3).

To implement the external magnetic field condition, a large cylindrical region was added to the geometry. The diameter of this cylinder is five times larger than the length of the cable, forming what is commonly referred to in electromagnetic modeling as the ''air'' domain—i.e., a non-magnetic, highly resistive medium [16], [34]. A mapped mesh using an edge selection technique was applied to the HTS regions in both the CORC and TSTC tapes, while a free tetrahedral mesh was used for the air domain. To satisfy convergence requirements, minimize meshing errors, and optimize computation time, different edge selection parameters were tested for both the outer layer and the inner former tapes as shown in Figure 1(b). A mesh sensitivity analysis was performed to evaluate the accuracy of AC loss calculations in both CORC and TSTC superconducting tapes. To ensure mesh-independent results, a configuration employing hexahedral elements was used, with each element's thickness set equal to be no greater than that of the HTS layer. The tape cross-section was then discretised into a control grid of 6×90 elements along the width and length, respectively, incorporating an additional diagonal edge for better capturing current redistribution.

The results obtained when discretizing the thickness of the HTS tapes into two and three equally sized elements (without diagonal edge) deviated, on average, by less than 9% and 4%, respectively, from those obtained with the coarser mesh (for the 20 mT and 100 mT applied magnetic fields). However, this came at the cost of a two- to four-fold increase in computing time relative to the baseline control grid. For instance, in the CORC-TSTC hybrid cable with a single HTS tape at the TSTC core, simulating a full AC excitation cycle at $B_a = 20$ mT required of approximately 2 computing hours, and about just 15 minutes more for $B_a = 100$ mT, when the constant J_c model is assumed. However, if instead, the actual magneto-angular anisotropy of the HTS tapes is accounted for via Equation 11, the computing time may triple or more (see Table 2), as the anisotropy factor ϵ_θ must be evaluated within each element and at every iteration so that $J_c(\mathbf{B}, \theta)$ is updated locally. This naturally adds considerable computational overhead, but returns results in much closer agreement with the

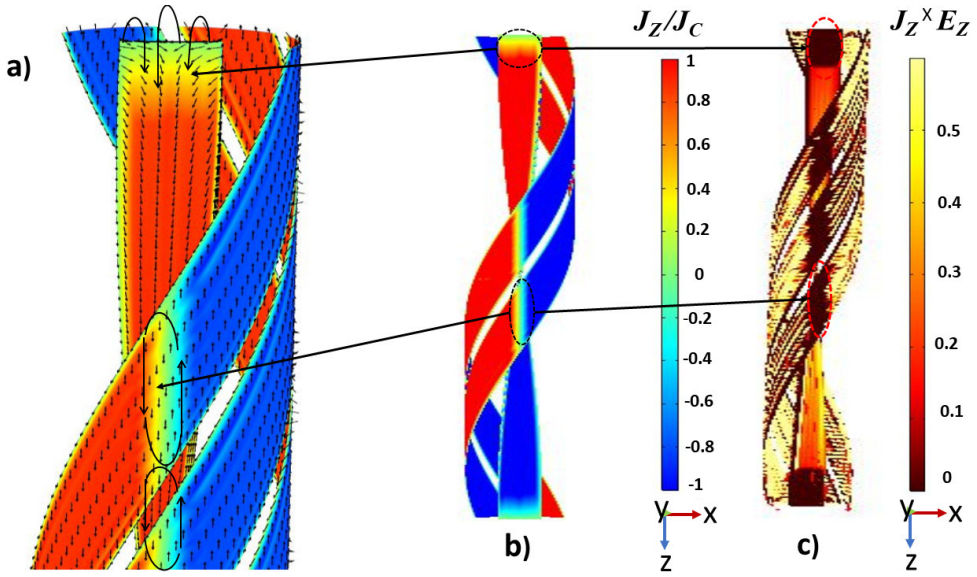

FIGURE 3. (a) Snapshot of the half the pitch length of the hybrid CORC–TSTC cable (by symmetry), using the TSTC pitch as a reference. The image shows complex magnetization current loops in both the CORC and TSTC layers under an applied magnetic field of 90 mT at 12.5 ms.(b) Full view of the cable's pitch length, providing context for the current distribution.(c) Identification of thermodynamically "cooler" regions within the cable, where flux-free core areas emerge due to opposing magnetization currents flowing in adjacent domains.

experimental evidence, as shown in Figure 4. Likewise, no significant improvements in accuracy were observed by further increasing the element density along the tape's width and length; however, numerical instabilities, particularly noticeable in the instantaneous energy loss curves for the CORC layers, were sometimes observed when using fewer than 5 elements across the width, or fewer than 80 along the length. Moreover, omitting the diagonal edge in the control mesh often led to convergence failures at field amplitudes as low as or beyond 20 mT, unless mesh-relative error magnitudes were tightly controlled to avoid spurious directional flips in field derivatives, essential for maintaining tangential continuity and physical consistency of the solution. For this reason, we recommended the control mesh configuration where the physics-controlled error and tolerance settings in COMSOL are left unaltered, as the lowest mesh quality acceptable for accurate results. This configuration yielded results within a 5% tolerance, for more than 90% of the experimental cases, indicating satisfactory convergence and affordable computing times. In contrast, applying a similar mesh resolution and using tetrahedral elements leads to a substantial increase in computation time ($>$ 300%) and, in some cases, non-convergent solutions. These issues were found to depend strongly on the applied magnetic field intensity and the degree of mesh homogeneity, highlighting the practical limitations of tetrahedral meshing for such high-gradient field problems. All computations were made using a standard HP Z2 Tower G5 Workstation equipped with 10 Intel Core i9-10900K processors at 3.6 GHz base clock-speed and 128 GB DDR4 memory, and on COMSOL Multiphysics 5.6.

TABLE 2. Sample of computing times attained with the control mesh for diverse CORC-TSTC hybrid cables referred at Figure 4.

TSTC*	B_a	Computing Time with J_c constant	Computing Time with $J_c(\mathbf{B},\theta)$
1	20 mT	01:58:48	06:44:49
1	50 mT	01:41:40	20:40:02
1	100 mT	02:14:35	15:22:26
2	20 mT	01:48:36	04:20:11
2	50 mT	01:47:52	13:06:11
2	100 mT	01:57:30	23:52:21
4	20 mT	04:27:59	04:54:43
4	50 mT	04:44:35	15:41:33
4	100 mT	04:20:22	18:28:02

* Number of HTS layers at the TSTC core. For all cases, six HTS tapes are considered for the outer CORC in the hybrid designs.

III. RESULTS AND DISCUSSION

In what follows, we turn our attention to the outcomes of the three-dimensional numerical approach introduced earlier, focusing on two key aspects of hybrid CORC–TSTC cable performance: the distribution of magnetization currents and the associated AC losses under varying configurations. The analysis begins with a detailed investigation of current density profiles across different cable geometries, followed by a comparative study of AC loss behaviour validated against experimental data. These results shed light on the electromagnetic response of these complex architectures and help to explore the extent to which hybrid designs can offer performance advantages over more conventional layouts.

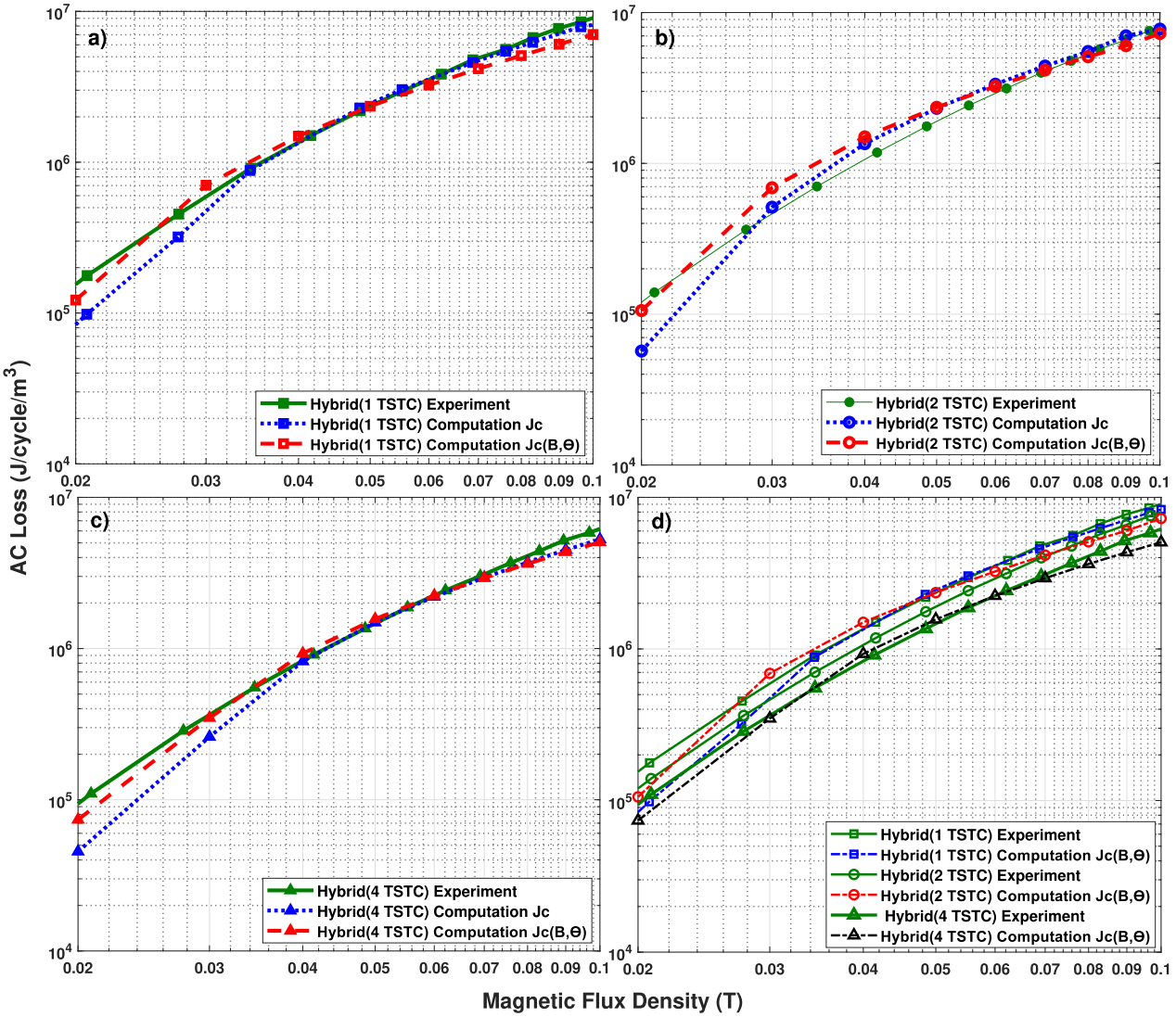

FIGURE 4. Comparison between the experimentally measured AC Losses and those obtained with our 3D model for CORC-TSTC hybrid cables comprised of: (a) Six tapes in the CORC layer + 1 tape for the TSTC inside the former; (b) Six tapes in the CORC layer + 2 tapes for the TSTC; (c) Six tapes in the CORC layer + 4 tapes for the TSTC. (d) Shows the AC Losses reduction according to the number of tapes in the TSTC at the CORC-TSTC hybrid cable.

A. MAGNETIZATION CURRENT DISTRIBUTION

We begin by examining the distribution of magnetization currents within the superconducting tapes for three cable configurations: the hybrid CORC–TSTC, a single-layer CORC, and a two-layer CORC, as illustrated in Figure 2. Shown are the normalized current density profiles, J_z/J_c, in the HTS tapes subjected to an externally applied sinusoidal magnetic field of 60 Hz and 90 mT amplitude, coherently with the experimental conditions at [27], and evaluated at 12.5 ms with the field oriented along the y-axis.

In particular, Figure 2(a) presents the current density distribution J_z/J_c for the hybrid CORC–TSTC cable, which comprises six HTS tapes in the CORC layer surrounding a TSTC core made of four stacked HTS tapes—resulting in a total of ten HTS tapes in the hybrid design. Figure 2(b) provides a zoomed-in view of the TSTC conductor, highlighting regions of interest such as tape edges and the twist section at half the pitch length. Similarly, Figure 2(c) depicts a likewise configuration regarding the end use of HTS tapes: a double-layer CORC cable composed of six HTS tapes in the outer layer and four in the inner layer, matching the total tape count of the hybrid prototype. Finally, Figure 2(d) presents the reference case of a single-layer CORC cable with six HTS tapes whose model has been previously validated against available experimental results [16], [43].

Interestingly, the current density distribution in the outer CORC layer of the hybrid CORC–TSTC cable closely resembles that of conventional HTS CORC cables. Specifically, it exhibits the classical left–right symmetry of positive and negative current lobes, consistent with the

Bean-like profiles observed in cylindrical wires subjected to transverse magnetic fields under zero-transport current conditions [49], [50]. A closer inspection of the 2G-HTS tape cross-section (see Figure 2(a)) confirms that each tape exhibits this characteristic distribution across its thickness, including clearly defined flux-free regions—highlighting the predictive power of our full 3D modeling approach.

It is worth emphasizing that such features cannot be resolved using reduced-dimensionality models, which underscores the strength of our approach in revealing a more detailed view of the system's physical response. For instance, in contrast to the behaviour observed in the CORC layer of the hybrid cable, the TSTC tapes within the same configuration exhibit markedly different current density patterns. While still governed by the principles of Bean's critical state model, their profiles resemble those of thin films exposed to magnetic fields aligned parallel (rather than perpendicular) to the tape surface. This behaviour is illustrated in Figure 2(a) and (b), where the normalized current density J_z/J_c in the TSTC core is strongly influenced by the varying field orientation along the twisted geometry.

Remarkably, the electromagnetic response of the CORC layers as a whole aligns well with Brandt's theoretical model for type-II superconductors under perpendicular magnetic fields [51]. Indeed, in Figure 2(b) we observe how the orientation of the applied magnetic field evolves along the twist pitch: at both ends of the pitch, the field is nearly perpendicular to the HTS tape surface, while at a quarter of the twist pitch length, it becomes nearly parallel—resulting in a distinct current penetration profile. This differs from the expected strip-like penetration under purely perpendicular field conditions, as predicted by Brandt, which would typically occur at half the twist pitch length. These results illustrate the complexity of real 3D current paths, which can only be captured through detailed numerical modeling (see Figure 3). Depending on the tape's geometry and the field orientation, magnetization currents form loops that close either across the tape's width and thickness—as observed in CORC cables—or along the tape's length and thickness—as observed in twisted TSTC tapes (see Figure 3(a)). The latter behaviour is consistent with our recent results for TSTC conductors [39]. It underscores the necessity of using fully 3D modeling to accurately resolve the local current density distributions in such hybrid superconducting cable architectures.

B. AC-LOSS ANALYSIS

To validate the reliability of our model prior to further analysis, we first compare the simulation results with available experimental data. In this case, magnetization losses serve as the key validation metric [27]. Thus, in Figure 4, we compare the calculated AC losses against the experimental measurements for all hybrid cable configurations, ranging from a hybrid cable with six HTS tapes in the CORC layer and one TSTC tape in the former, as a default cable layout, up to a configuration with four TSTC tapes in the former (see Figure 4(a–c)).

The analysis includes simulation results using both a constant critical current density $J_c = J_{c0}$ (blue dotted line), and a magneto-angular-dependent $J_c(\mathbf{B}/\theta)$ (red dashed line), while the experimental results are represented by green solid lines. Clearly, neglecting the magneto-angular anisotropy of the HTS tapes can lead to a weak but noticeable underestimation of the AC losses at low magnetic fields. This discrepancy arises due to the expected invariance of the norm of J_c across the length of the element edges (when assumed constant), reducing thereby the spatial resolution within the finite element, an effect that is mitigated when the $J_c(\mathbf{B}, \theta)$ function is used, albeit at the cost of a substantial increase in computing time (see Table 2). Yet, as the magnetic field penetrates more deeply into the HTS tapes, the area where magnetization currents are induced becomes more uniformly distributed with one or another approach. Then, as it is precisely the local movement of the magnetization currents that, in response to changes in the external magnetic field, gives rise to hysteretic losses, the differences between the models diminish at higher field amplitudes (see Figure 4), except in terms of computational cost.

In more detail, for the first case, i.e., the hybrid cable with a single TSTC tape (Figure 4(a)), our 3D model with constant J_c tends to underestimate the AC losses at the lowest magnetic field amplitudes (10)–20 mT) relative to the experimental data. However, as noted above, this discrepancy becomes negligible as the magnetic field increases (30-100 mT), where both modeling approaches align well with the experimental measurements. The low-field deviation, primarily observed in the case with a single HTS tape in the TSTC core, persists even when the $J_c(\mathbf{B}/\theta)$ function is used, and could be therefore attributed to the relatively coarse discretization across the tape thickness, in accordance with our mesh sensitivity analysis. In this context, it is worth reminding that while increasing mesh density would indeed improve local accuracy, particularly when accounting for the tape's magneto angular anisotropy, it could also substantially raise the computation time. As a result, a trade-off must be observed, especially when other sources of uncertainty may arise from extrinsic factors such as experimental instrumentation or the actual accuracy of the $J_c(\mathbf{B}, \theta)$ approach for each of the HTS tapes in the real cable. In particular, consider that, in practice, J_c curves are typically obtained from flat tape specimens before any winding or twisting, which may alter their effective behaviour. On the other hand, differences attributed to the imperfectly predicted field penetration profiles decrease as the applied field increases because field gradients within the sample are less relevant and one may even evaluate losses via Bean's model. Thus, given the relatively minor deviation observed, the present model with the established control mesh is considered sufficiently accurate for the purposes of this study.

Similarly, Figure 4(b) presents results for a hybrid cable with the same CORC layer but with two HTS tapes in the

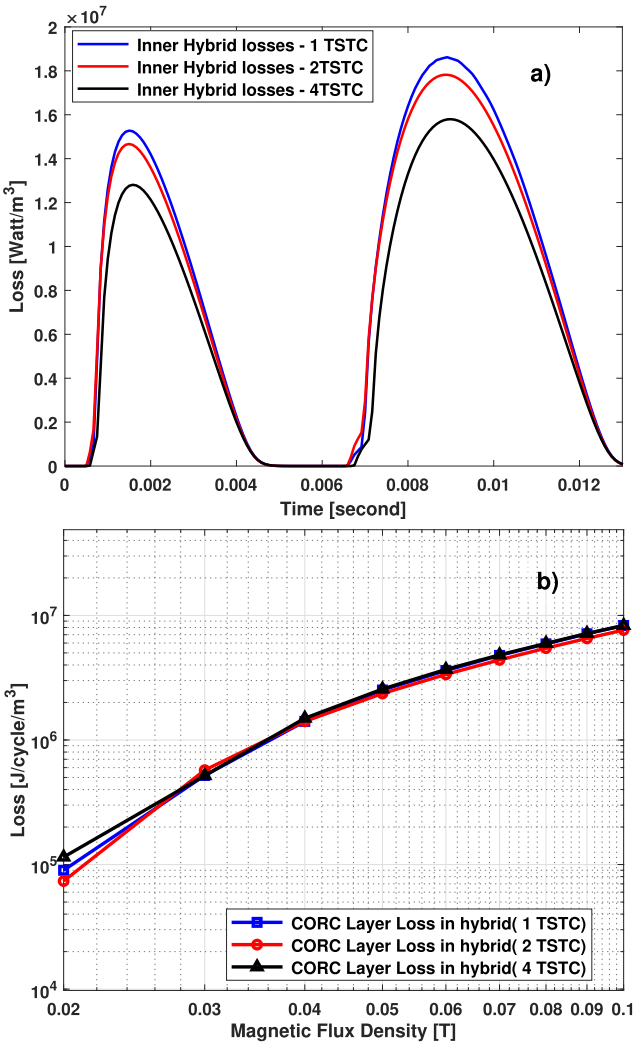

FIGURE 5. (a) Illustration of the reduction of instantaneous AC losses for the inner layer (TSTC) in the hybrid cable as the number of stacked tapes increases, under applied AC magnetic field of amplitude 90 mT. (b) Demonstration of the negligible influence of the number of stacked tapes in the TSTC within the cable former on the AC losses of the hybrid cable outer layer (CORC layer).

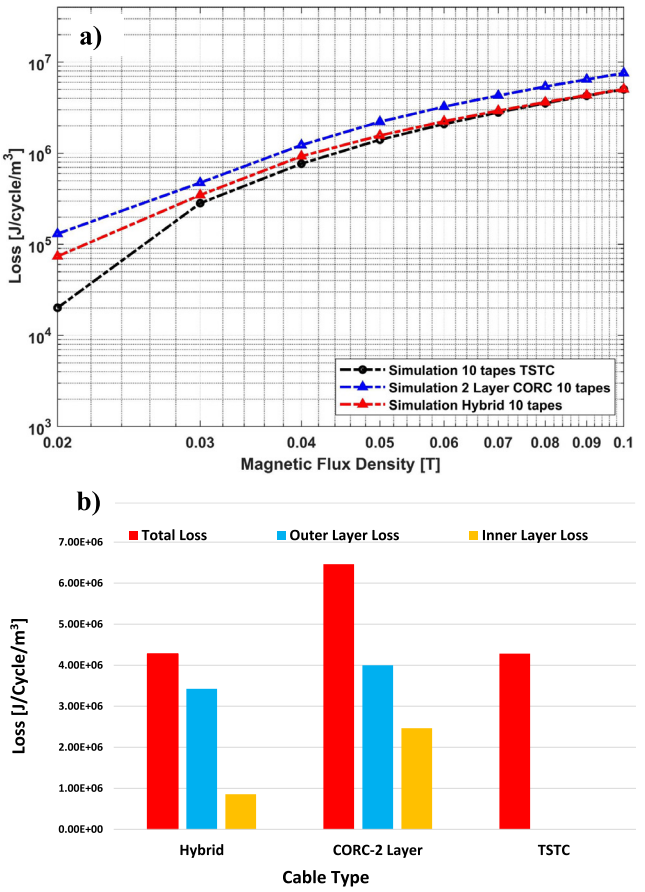

FIGURE 6. (a) Comparison between the AC losses for a bi-layer CORC cable with four 2G-HTS tapes in the inner layer and six in the outer layer, with those of an equivalent TSTC cable with ten 2G-HTS tapes, and with those for a hybrid cable with 4 tapes within the TSTC-core and 6 tapes at the outer CORC layer. (b) Illustration of the AC losses of layers in different cable structures, Hybrid, Bi-Layer CORC and TSTC cable under applied magnetic field 90 mT.

TSTC region. The analysis is then extended to the case of four TSTC tapes, shown in Figure 4(c). As summarized in Figure 4(d), the magnetization losses in the hybrid cable decrease as the number of TSTC tapes inside the former increases, a trend confirmed by both experimental and simulated data. This effect arises from the magnetic shielding generated by the outer layers of the TSTC cable, which leads to a twofold outcome. First, the magnetic field penetrating each HTS layer in the TSTC is progressively attenuated, resulting in a corresponding reduction in their magnetization losses. Second, as the inner layers experience a weaker magnetic field, the degradation of their critical current density, governed by the magneto-angular dependence $J_c(\mathbf{B}, \theta)$ is less pronounced [39]. Specifically, for the CORC-TSTC hybrid cables considered at Figure 4, the difference in AC losses between the hybrid cable with one TSTC tape and that with four TSTC tapes at an applied field of 0.1 T, is of 36% according to experimental measurements, and 38% in the 3D model. The average reduction across the entire field range is 7.11% experimentally, and 8.7% in the simulation. Furthermore, to evaluate whether increasing the number of TSTC layers within the hybrid cable influences the AC losses in the outer CORC layer, we calculated the losses for the CORC layer alone using our 3D model (see Figure 5(b)). As shown, increasing the number of TSTC tapes does not affect the AC losses in the outer layer. This indicates that the total AC losses in the hybrid cable are primarily dominated by the CORC layers as illustrated in Figure 5(a), and that the observed reduction in total losses (see Figure 4(d)) is attributed to the lower field penetration on the TSTC core, what is in agreement with our previous observations in single TSTC configurations [39].

Finally, we consider three configurations, each containing the same total number of HTS tapes (ten), but arranged differently: (1) a bi-layer CORC cable with four tapes in the inner layer and six in the outer layer, (2) a TSTC cable with

ten stacked tapes, and (3) a hybrid cable with four tapes in the TSTC core and six in the outer CORC layer. The AC losses per unit volume for these configurations are shown in Figure 6(a), and the distribution of losses between outer and inner layers is presented in Figure 6(b). In all cases, an AC magnetic field of amplitude 90 mT is applied.

As seen in Figure 6(b), the outer CORC layer consistently dominates the AC loss contribution in both the hybrid and bi-layer CORC cables. However, the hybrid configuration achieves a noticeably lower total loss compared to the bi-layer CORC cable, despite using the same number of tapes. This reduction arises from the significantly lower losses in the TSTC core compared to the inner CORC layer in the bi-layer cable. In contrast, the TSTC cable with ten stacked tapes shows the lowest total AC losses among the three configurations. However, the difference relative to the hybrid cable becomes negligible at higher applied magnetic fields, as the loss contribution is more evenly distributed owing to the uniform tape stacking. These results indicate that hybrid designs achieve a favourable balance, preserving structural complexity and shielding advantages, while reducing total AC losses more effectively than pure CORC cables, even when compared with pure TSTC designs, except at very low fields ($<$ 30 mT), a region where the TSTC clearly outperforms.

IV. CONCLUSION

In this study, a fully three-dimensional electromagnetic modeling framework for hybrid CORC–TSTC superconducting cables has been presented, offering new insights into their magnetization behaviour and AC loss characteristics—validated comprehensively against recent experimental observations. A distinguishing feature of the proposed model is its foundation on overcoming the limitations of prior approaches, particularly those relying on reduced-dimensionality approximations such as the T–A formulation. While such gauge-based methods are computationally efficient, they fail to capture key local electromagnetic phenomena, including flux-free cores and internal shielding effects, which are essential for accurately modeling twisted and helically wound composite geometries.

The modeling strategy was validated through close comparison with experimental measurements of magnetization losses across various CORC-TSTC hybrid cable configurations. A detailed analysis of magnetization current density distributions revealed that the outer CORC layer dominates the AC loss profile, while the internal TSTC tapes benefit from the stronger pinning mechanism characteristic of thin films in a parallel magnetic field [39], [51]. In the hybrid cable, the CORC layer exhibited a ''*Bean-like*'' current pattern consistent with seminal models for cylindrical wires under perpendicular magnetic fields [49], [52], [53], which, when examined in greater detail, have revealed the 3D structure of current loops that close across the tape's width and thickness. In contrast, the TSTC conductor forms current loops along its length and thickness, resembling the current profiles characteristic of finite thin films subjected to longitudinal magnetic field components. These results not only offer valuable physical insight but also confirm the capability of the 3D model to resolve intricate local current behaviours that lie beyond the reach of reduced-order formulations. As such, they should not be conflated with simplified approaches such as the T–A formulation, where the tape thickness is neglected and spatial variations of electromagnetic quantities across the superconducting cross-section are inherently omitted, effectively overlooking the internal structure and depth-dependent physics of the superconductor.

Notably, while the CORC layer contributes the majority of the total AC losses, the inclusion of a TSTC core substantially improves overall efficiency without affecting the loss profile of the outer layer—underscoring the hybrid design's potential to reduce losses without increasing cable complexity or footprint. Furthermore, when comparing three functionally equivalent designs—(i) a two-layer CORC cable, (ii) a ten-tape TSTC cable, and (iii) a hybrid CORC–TSTC cable with the same total number of tapes—the hybrid configuration emerges as a superior trade-off. It demonstrates lower total AC losses than the two-layer CORC cable and comparable loss levels to the TSTC cable, while preserving the mechanical and electrical advantages of the CORC geometry. These findings establish the hybrid architecture as a compelling option for applications demanding both electromagnetic performance and design flexibility. The hybrid CORC–TSTC topology not only harnesses the complementary features of its constituent components but also presents a scalable platform for future innovation. The modeling framework developed here can be readily extended to support investigations involving dynamic load conditions, transport currents, or integration into magnet coils and cable-in-conduit systems, with applicability across fusion energy, aerospace, and grid-scale superconducting technologies. In the latter, although no experimental measurements of AC losses under transport current conditions are yet available for CORC-TSTC hybrid cables, the numerical model presented in this study provides a robust foundation for baseline OPEX estimations, particularly when the cable is not intended for fault current limiting applications. In scenarios where quench behaviour becomes relevant, a more comprehensive numerical framework would be required, i.e., one that concurrently solves Maxwell's equations alongside Newton's heat transfer equation, thereby enabling analysis of key parameters such as minimum quench energy and normal zone propagation velocity. However, importantly, the practical limitations surrounding the fabrication of large-scale HTS cable prototypes, combined with the scarcity of experimental facilities capable of measuring total (i.e., calorimetric) AC losses over representative cable lengths, underscore the timeliness and value of models like the one developed here, and why magnetization experiments are first considered. Thus, now that our model has been validated against the world's first magnetization loss data for hybrid

CORC–TSTC cables, our numerical framework is well-positioned to support future studies involving transport current AC losses, which will be addressed in a forthcoming publication.

REFERENCES

[1] H. S. Ruiz, J. Hänisch, M. Polichetti, A. Galluzzi, L. Gozzelino, D. Torsello, S. Milošević-Govedarović, J. Grbović-Novaković, O. V. Dobrovolskiy, W. Lang, G. Grimaldi, A. Crisan, P. Badica, A. M. Ionescu, P. Cayado, R. Willa, B. Barbiellini, S. Eley, and A. Badía–Majós, "Critical current density in advanced superconductors," *Prog. Mater. Sci.*, vol. 155, Jan. 2026, Art. no. 101492, doi: 10.1016/j.pmatsci.2025.101492.

[2] M. D. Sumption, M. Majoros, and E. W. Collings, "AC losses in superconducting materials, wires, and tapes," in *Handbook of Superconductivity*. Boca Raton, FL, USA: CRC Press, 2022, pp. 238–250.

[3] T. A. Coombs, Q. Wang, A. Shah, J. Hu, L. Hao, I. Patel, H. Wei, Y. Wu, T. Coombs, and W. Wang, "High-temperature superconductors and their large-scale applications," *Nature Rev. Electr. Eng.*, vol. 1, no. 12, pp. 788–801, Nov. 2024, doi: 10.1038/s44287-024-00112-y.

[4] S. Y. Gao, X. Y. Tan, H. Zhang, F. G. Cai, X. S. Yang, J. Jiang, B. Y. Shen, and Y. Zhao, "Reducing magnetization AC loss in twisted-stacked HTS cables," *IEEE Trans. Appl. Supercond.*, vol. 35, no. 4, pp. 1–8, Jun. 2025, doi: 10.1109/TASC.2025.3555643.

[5] Y. Li, L. Jiang, M. Xie, J. Yu, L. Qian, K. Xu, M. Chen, and Y. Wang, "Advancements and challenges in power cable laying," *Energies*, vol. 17, no. 12, p. 2905, Jun. 2024. [Online]. Available: https://www.mdpi.com/1996-1073/17/12/2905

[6] G. E. Gardner, "AC and DC power transmission," *Electron. Power*, vol. 32, no. 2, pp. 171, Feb. 1986.

[7] S. Aboudrar, A. Allais, K. Allweins, K. Berger, G. Bouvier, J. Capron, H. Caron, D. Ferandelle, L. Gervaise, R. Goncalves, G. Hajiri, A. Jazzar, N. Lallouet, L. Quéval, and B. West, "Qualification of the SuperRail HTS cable system," *IEEE Trans. Appl. Supercond.*, vol. 35, no. 5, pp. 1–6, Aug. 2025, doi: 10.1109/TASC.2025.3538520.

[8] D. Willén, M. Sedén, M. Pitzer, V. Roudriges-Zermeno, C. Thidemann, J. Kunert, D. D. Tjahjanto, C. Frohne, O. Holte, C. Wolff, W. Prusseit, C. Hintze, R. Bach, P. Mansheim, W. T. B. de Sousa, M. Noe, A. Alekseev, P. Michalek, and R. Prinz, "Development of the superlink HTS cable system for implementation in Munich," *IEEE Trans. Appl. Supercond.*, vol. 35, no. 5, pp. 1–8, Aug. 2025, doi: 10.1109/TASC.2025.3553829.

[9] M. A. Green, "A retrospective on how cryostats have changed with cryostat use and the cooling methods used to keep superconducting magnets cold," *IOP Conf. Ser., Mater. Sci. Eng.*, vol. 1301, no. 1, May 2024, Art. no. 012154, doi: 10.1088/1757-899x/1301/1/012154.

[10] W. Goldacker, R. Nast, G. Kotzyba, S. I. Schlachter, A. Frank, B. Ringsdorf, C. Schmidt, and P. Komarek, "High current DyBCO-ROEBEL assembled coated conductor (RACC)," *J. Phys., Conf. Ser.*, vol. 43, pp. 901–904, Jun. 2006, doi: 10.1088/1742-6596/43/1/220.

[11] W. Goldacker, A. Frank, R. Heller, S. I. Schlachter, B. Ringsdorf, K.-P. Weiss, C. Schmidt, and S. Schuller, "ROEBEL assembled coated conductors (RACC): Preparation, properties and progress," *IEEE Trans. Appl. Supercond.*, vol. 17, no. 2, pp. 3398–3401, Jun. 2007, doi: 10.1109/TASC.2007.899417.

[12] W. Goldacker, F. Grilli, E. Pardo, A. Kario, S. I. Schlachter, and M. Vojenčiak, "Roebel cables from REBCO coated conductors: A one-century-old concept for the superconductivity of the future," *Superconductor Sci. Technol.*, vol. 27, no. 9, Sep. 2014, Art. no. 093001, doi: 10.1088/0953-2048/27/9/093001.

[13] S. S. Fetisov, V. V. Zubko, S. Yu Zanegin, A. A. Nosov, S. M. Ryabov, and V. S. Vysotsky, "Study of the first Russian triaxial HTS cable prototypes," *IEEE Trans. Appl. Supercond.*, vol. 27, no. 4, pp. 1–5, Jun. 2017, doi: 10.1109/TASC.2017.2652854.

[14] D. C. van der Laan, J. D. Weiss, and D. M. McRae, "Status of CORC cables and wires for use in high-field magnets and power systems a decade after their introduction," *Superconductor Sci. Technol.*, vol. 32, no. 3, Mar. 2019, Art. no. 033001, doi: 10.1088/1361-6668/aafc82.

[15] J. Goo, J.-W. Han, S. Lee, W.-S. Kim, K. Choi, and J.-K. Lee, "Magnetization loss of CORC with various configurations of 2G HTS strands," *IEEE Trans. Appl. Supercond.*, vol. 31, no. 5, pp. 1–5, Aug. 2021, doi: 10.1109/TASC.2021.3067810.

[16] M. U. Fareed, M. Kapolka, B. C. Robert, M. Clegg, and H. S. Ruiz, "3D FEM modeling of *CORC* commercial cables with Bean's like magnetization currents and its AC-losses behavior," *IEEE Trans. Appl. Supercond.*, vol. 32, no. 4, pp. 1–5, Jun. 2022, doi: 10.1109/TASC.2022.3145309.

[17] W. H. Fietz, M. J. Wolf, A. Preuss, R. Heller, and K.-P. Weiss, "High-current HTS cables: Status and actual development," *IEEE Trans. Appl. Supercond.*, vol. 26, no. 4, pp. 1–5, Jun. 2016, doi: 10.1109/TASC.2016.2517319.

[18] X. Li, D. Song, Y. Wu, Y. Liu, W. Yang, and R. Macian-Juan, "Current-carrying capability and magnetic behavior of the HTS twisted stacked-tape conductor cable for the compact fusion reactor," *IEEE Trans. Appl. Supercond.*, vol. 32, no. 4, pp. 1–5, Jun. 2022, doi: 10.1109/TASC.2021.3138710.

[19] K. Choi, J. Han, J.-K. Lee, and W.-S. Kim, "Magnetization loss measurement of twisted stacked tape cable and comparison with CORC," *IEEE Trans. Appl. Supercond.*, vol. 33, no. 5, pp. 1–5, Aug. 2023, doi: 10.1109/TASC.2023.3243537.

[20] J. Yang, C. Li, M. Tian, S. Liu, B. Shen, L. Hao, Y. Ozturk, and T. Coombs, "Analysis of AC transport loss in conductor on round core cables," *J. Supercond. Novel Magnetism*, vol. 35, no. 1, pp. 57–63, Jan. 2022, doi: 10.1007/s10948-021-06031-5.

[21] M. Vojenčiak, A. Kario, B. Ringsdorf, R. Nast, D. C. van der Laan, J. Scheiter, A. Jung, B. Runtsch, F. Gömöry, and W. Goldacker, "Magnetization AC loss reduction in HTS CORC cables made of striated coated conductors," *Superconductor Sci. Technol.*, vol. 28, no. 10, Oct. 2015, Art. no. 104006, doi: 10.1088/0953-2048/28/10/104006.

[22] J. Han, W.-S. Kim, K. Choi, and J.-K. Lee, "Magnetization loss of multi-layered CORC according to various winding types," *IEEE Trans. Appl. Supercond.*, vol. 32, no. 6, pp. 1–5, Sep. 2022, doi: 10.1109/TASC.2022.3157800.

[23] Y. Wu, Z. Chen, G. Geng, J. Fang, and Y. Liu, "AC losses analysis of HTS composite conductors with different current ramp rates," *IEEE Trans. Appl. Supercond.*, vol. 29, no. 2, pp. 1–5, Mar. 2019, doi: 10.1109/TASC.2019.2894847.

[24] M. Takayasu, L. Chiesa, L. Bromberg, and J. V. Minervini, "HTS twisted stacked-tape cable conductor," *Superconductor Sci. Technol.*, vol. 25, no. 1, Jan. 2012, Art. no. 014011, doi: 10.1088/0953-2048/25/1/014011.

[25] M. Takayasu, L. Chiesa, L. Bromberg, and J. V. Minervini, "Cabling method for high current conductors made of HTS tapes," *IEEE Trans. Appl. Supercond.*, vol. 21, no. 3, pp. 2340–2344, Jun. 2011, doi: 10.1109/TASC.2010.2094176.

[26] M. Takayasu, L. Chiesa, L. Bromberg, and J. V. Minervini, "Electrical and mechanical characteristics of HTS twisted stacked-tape cable conductor," *IEEE Trans. Appl. Supercond.*, vol. 27, no. 4, pp. 1–5, Jun. 2017, doi: 10.1109/TASC.2017.2652307.

[27] M. Yoon, M. Lee, J.-K. Lee, K. Choi, and W.-S. Kim, "Experimental study of magnetization loss by external magnetic field in CORC-TSTC hybrid composite conductor," *IEEE Trans. Appl. Supercond.*, vol. 34, no. 5, pp. 1–5, Aug. 2024, doi: 10.1109/TASC.2023.3347376.

[28] Z. S. Hartwig et al., "VIPER: An industrially scalable high-current high-temperature superconductor cable," *Superconductor Sci. Technol.*, vol. 33, no. 11, Nov. 2020, Art. no. 11LT01, doi: 10.1088/1361-6668/abb8c0.

[29] S. Fu, M. Qiu, J. Zhu, H. Zhang, J. Gong, X. Zhao, W. Yuan, and J. Guo, "Numerical study on AC loss properties of HTS cable consisting of YBCO coated conductor for HTS power devices," *IEEE Trans. Appl. Supercond.*, vol. 28, no. 4, pp. 1–5, Jun. 2018, doi: 10.1109/TASC.2018.2816819.

[30] F. Grilli, E. Pardo, A. Morandi, F. Gömöry, M. Solovyov, V. M. R. Zermeño, R. Brambilla, T. Benkel, and N. Riva, "Electromagnetic modeling of superconductors with commercial software: Possibilities with two vector potential-based formulations," *IEEE Trans. Appl. Supercond.*, vol. 31, no. 1, pp. 1–9, Jan. 2021, doi: 10.1109/TASC.2020.3013028.

[31] Y. Wang, M. Zhang, F. Grilli, Z. Zhu, and W. Yuan, "Study of the magnetization loss of CORC cables using a 3D T–A formulation," *Superconductor Sci. Technol.*, vol. 32, no. 2, Jan. 2019, Art. no. 025003, doi: 10.1088/1361-6668/aaf011.

[32] S. Zhang, K. Wang, J. Yan, and Y. Gao, "Magnetization loss of CORC cables under axial tensile loading," *Phys. C, Supercond. Appl.*, vol. 603, Dec. 2022, Art. no. 1354174.

[33] L. Lai and C. Gu, "J model for studying AC magnetization loss in 3D cable structures," *Superconductor Sci. Technol.*, vol. 35, no. 4, Feb. 2022, Art. no. 045008, doi: 10.1088/1361-6668/ac55f4.

[34] J. Sheng, M. Vojenciak, R. Terzioglu, L. Frolek, and F. Gömöry, "Numerical study on magnetization characteristics of superconducting conductor on round core cables," *IEEE Trans. Appl. Supercond.*, vol. 27, no. 4, pp. 1–5, Jun. 2017, doi: 10.1109/TASC.2016.2632901.
[35] F. London and H. London, "The electromagnetic equations of the supraconductor," *Proc. Roy. Soc. London. Ser. A Math. Phys. Sci.*, vol. 149, no. 866, pp. 71–88, 1935, doi: 10.1098/rspa.1935.0048.
[36] W. Meissner and R. Ochsenfeld, "Ein neuer effekt bei eintritt der supraleitfaehigkeit," *Die Naturwissenschaften*, vol. 21, no. 44, pp. 787–788, Nov. 1933.
[37] A. A. Abrikosov, "On the magnetic properties of superconductors of the second group," *Zh Eksperim.I Teor Fiz*, vol. 32, pp. 1174–1182, Jan. 1956. [Online]. Available: http://www.jetp.ac.ru/cgi-bin/e/index/e/5/6/p1174?a=list
[38] M. Clegg and H. S. Ruiz, "3D electromagnetic assessment of bended CORC cables," *J. Appl. Phys.*, vol. 136, no. 3, Jul. 2024, Art. no. 033902, doi: 10.1063/5.0218241.
[39] M. Clegg, H. N. H. Al-Ssalih, and H. S. Ruiz, "Magnetization losses of transposed stacked tape conductors under AC transverse magnetic fields," *IEEE Access*, vol. 13, pp. 84013–84023, 2025, doi: 10.1109/ACCESS.2025.3566645.
[40] K. Osamura, S. Machiya, and D. P. Hampshire, "Mechanism for the uniaxial strain dependence of the critical current in practical REBCO tapes," *Superconductor Sci. Technol.*, vol. 29, no. 6, pp. 65019–65035, Jun. 2016, doi: 10.1088/0953-2048/29/6/065019.
[41] B. Shen, F. Grilli, and T. Coombs, "Overview of H-formulation: A versatile tool for modeling electromagnetics in high-temperature superconductor applications," *IEEE Access*, vol. 8, pp. 100403–100414, 2020, doi: 10.1109/ACCESS.2020.2996177.
[42] M. Zhang and T. A. Coombs, "3D modeling of high-tcsuperconductors by finite element software," *Superconductor Sci. Technol.*, vol. 25, no. 1, Jan. 2012, Art. no. 015009, doi: 10.1088/0953-2048/25/1/015009.
[43] M. Clegg, M. Kapolka, and H. S. Ruiz, "Impact of the magneto angular dependence of the critical current density in CORC cables," *IEEE Trans. Appl. Supercond.*, vol. 32, no. 6, pp. 1–6, Sep. 2022, doi: 10.1109/TASC.2022.3153751.
[44] Y. B. Kim, C. F. Hempstead, and A. R. Strnad, "Critical persistent currents in hard superconductors," *Phys. Rev. Lett.*, vol. 9, no. 7, pp. 306–309, Oct. 1962, doi: 10.1103/physrevlett.9.306.
[45] P. M. Leys, M. Klaeser, F. Schleissinger, and T. Schneider, "Analysis of the anisotropic critical current behaviour of HTS coated conductors," *J. Phys., Conf. Ser.*, vol. 507, no. 2, May 2014, Art. no. 022013, doi: 10.1088/1742-6596/507/2/022013.
[46] X. Zhang, Z. Zhong, H. S. Ruiz, J. Geng, and T. A. Coombs, "General approach for the determination of the magneto-angular dependence of the critical current of YBCO coated conductors," *Superconductor Sci. Technol.*, vol. 30, no. 2, Feb. 2017, Art. no. 025010, doi: 10.1088/1361-6668/30/2/025010.
[47] M. Clegg and H. S. Ruiz, "Electromagnetic analysis and AC losses of triaxial cables with multiple 2G-HTS layers per phase," *Superconductivity*, vol. 5, Mar. 2023, Art. no. 100039, doi: 10.1016/j.supcon.2023.100039.
[48] A. Stenvall, M. Siahrang, F. Grilli, and F. Sirois, "Computation of self-field hysteresis losses in conductors with helicoidal structure using a 2D finite element method," *Superconductor Sci. Technol.*, vol. 26, no. 4, Apr. 2013, Art. no. 045011, doi: 10.1088/0953-2048/26/4/045011.
[49] H. S. Ruiz, A. Badía-Majós, Y. A. Genenko, H. Rauh, and S. V. Yampolskii, "Superconducting wire subject to synchronous oscillating excitations: Power dissipation, magnetic response, and low-pass filtering," *Appl. Phys. Lett.*, vol. 100, no. 11, Mar. 2012, Art. no. 112602, doi: 10.1063/1.3693614.
[50] H. S. Ruiz, A. Badia-Majos, Y. A. Genenko, and S. V. Yampolskii, "Strong localization of the density of power losses in type-II superconducting wires," *IEEE Trans. Appl. Supercond.*, vol. 23, no. 3, 2013, Art. no. 8000404, doi: 10.1109/TASC.2012.2232695.
[51] E. H. Brandt, "Superconductors of finite thickness in a perpendicular magnetic field: Strips and slabs," *Phys. Rev. B, Condens. Matter*, vol. 54, no. 6, pp. 4246–4264, Aug. 1996, doi: 10.1103/physrevb.54.4246.
[52] M. Ashkin, "Flux distribution and hysteresis loss in a round superconducting wire for the complete range of flux penetration," *J. Appl. Phys.*, vol. 50, no. 11, pp. 7060–7066, Nov. 1979, doi: 10.1063/1.325866.
[53] B. C. Robert and H. S. Ruiz, "Magnetic characteristics and AC losses of DC type-II superconductors under oscillating magnetic fields," *Superconductor Sci. Technol.*, vol. 31, no. 3, Feb. 2018, Art. no. 035006, doi: 10.1088/1361-6668/aaa823.

HASAN N. H. AL-SSALIH received the degree in electrical engineering and the M.Sc. degree in neural fuzzy control for induction machines from the University of Basra, Iraq, in 2002 and 2006, respectively. He is currently pursuing the Ph.D. degree in electrical engineering with the University of Leicester, U.K. He is a Chief Engineer with the Electrical Engineering Division, Iraq's Southern Fertilizer State Company (SFSC). From 2003 to 2010, he was a Senior Electrical Engineer in the generation and distribution of electrical power stations (132 KV to 11 KV and 6.6 KV) with SFSC. Since then, he has been a Chief Inspection Engineer for Electric Inspection Laboratories, specializing in high-tension and low-tension equipment and protective relays.

MATTHEW CLEGG received the master's degree in engineering and the Ph.D. degree in applied superconductivity and power systems from the University of Leicester, U.K., in 2020 and 2024, respectively. He is currently with the Distribution Systems Operator Insights Team, U.K. Power Networks, London, creating smart solutions to facilitate access to flexible connections in a whole system approach collaboration with U.K. National Energy System Operator (NESO).

ANTONIO BADÍA-MAJÓS received the Ph.D. degree in physics from the University of Zaragoza, Spain, in 1993. He is the Head of the School of Condensed Matter Physics, University of Zaragoza, Spain. He is a Full Professor and a member of the Institute of Nanoscience and Materials of Aragón (INMA). He has authored over 70 scientific papers in this field and a monographic book titled *Macroscopic Superconducting Phenomena*. He works actively to promote superconductivity through educational materials and outreach activities. His research has focused on superconducting materials, mainly contributing to several phenomenological theories, such as the critical state model.

HAROLD S. RUIZ received the Diploma degree in physics and the M.Sc. degree in condensed matter physics and superconductivity from the National University of Colombia, in 2004 and 2007, respectively, and the M.Sc. degree in physical technologies and the Ph.D. (cum laude) and European Doctorate in applied superconductivity from the University of Zaragoza, Spain, in 2008 and 2012, respectively. He is the Head of the Green Energy and Transport (GrEaT) Research Group, Electrical Engineering Division, University of Leicester, U.K. He is a Senior Fellow of the Higher Education Academy, U.K., and leads the research topic of applied superconductivity both at the University of Leicester and U.K. National Space Park Leicester. Before joining the University of Leicester, in 2015, he was with the Center for Advanced Power Systems, Florida State University, USA, and the Center for Advanced Photonics and Electronics Systems, University of Cambridge, U.K. He has co-authored more than ten funded research projects accounting for circa 3.5M (USD), published more than 60 scientific papers in this field, and leads the largest of the four specialized workgroups within European COST Action CA19108, Hi-Scale, which encompass about 140 senior researchers focused on the advancement of applied superconductivity, from materials to devices.